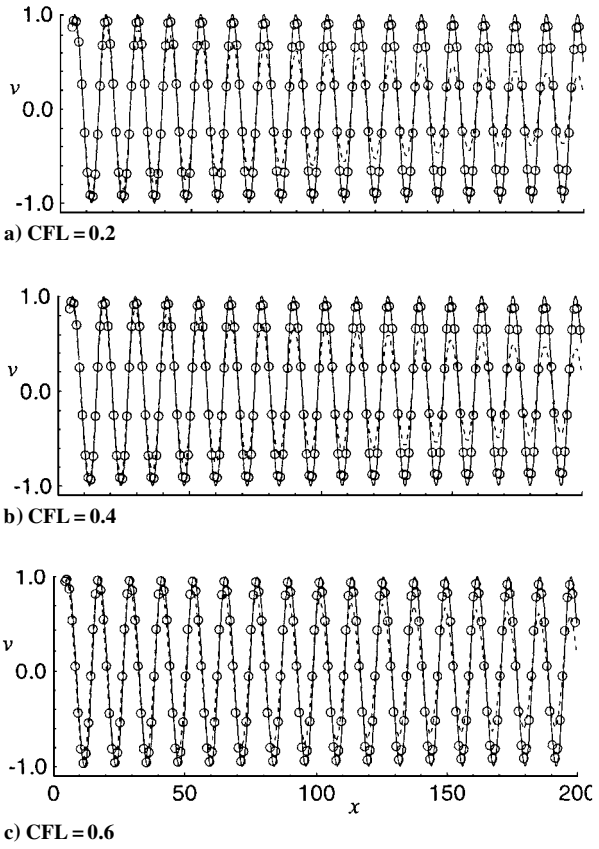


**Fig. 3 Comparisons of the resolution of the schemes for various CFL numbers (——, exact; - - - -, ENO3; and ○, ENO3–ACM).**

shows less diffusive behavior than ENO3 without the ACM for all CFL values considered.

## Conclusions

High-order terms in MFA-type ENO schemes are correctly derived in this Note. The scheme is tested for the positive-and negative-propagating waves, which is essential to calculate the Euler equations. The correct formulation is also important in the extension to higher-order schemes. To enhance the resolution of the ENO3, the ACM is successfully employed to the MFA–ENO3 scheme. It is shown that the MFA–ENO with the ACM gives numerical solutions of high-order accuracy and high resolution near discontinuity surfaces in flows and regions of small-amplitude acoustic waves. Finally, we conclude that the proposed scheme of ENO3 with the ACM is useful in problems involving acoustic waves with discontinuities.

## References

[1]Montagne, J. L., Yee, H. C., and Vinokur, M., "Comparative Study of High-Resolution Shock-Capturing Schemes for a Real Gas," *AIAA Journal*, Vol. 27, No. 10, 1989, pp. 1332–1346.

[2]Tam, C. K. W., "Computational Aeroacoustics Issues and Methods," AIAA Paper 95-0677, 1995.

[3]Kim, J. W., and Lee, D. J., "Optimized Compact Finite Difference Schemes with Maximum Resolution," *AIAA Journal*, Vol. 34, No. 5, 1995, pp. 887–893.

[4]Kim, J. W., and Lee, D. J., "Numerical Simulation of Nonlinear Waves Using Optimized High-Order Compact Schemes," *CFD Journal*, Vol. 5, No. 3, 1997, pp. 283–300.

[5]Harten, A., and Osher, S., "Uniformly High-Order Accurate Non-Oscillatory Schemes, I," *SIAM Journal on Numerical Analysis*, Vol. 24, No. 2, 1987, pp. 279–309.

[6]Shu, C.-W., and Osher, S., "Efficient Implementation of Essentially Non-Oscillatory Shock-Capturing Schemes," *Journal of Computational Physics*, Vol. 77, 1988, pp. 439–471.

[7]Casper, J., "Finite Volume Implementation of High-Order Essentially Nonoscillatory Schemes in Two-Dimensions," *AIAA Journal*, Vol. 30, No. 12, 1992, pp. 2829–2835.

[8]Yang, J. Y., "Third-Order Nonoscillatory Schemes for the Euler Equations," *AIAA Journal*, Vol. 29, No. 10, 1991, pp. 1611–1618.

[9]Yang, J. Y., and Hsu, C. A., "High-Resolution, Nonoscillatory Schemes for Unsteady Compressible Flows," *AIAA Journal*, Vol. 30, No. 6, 1992, pp. 1570–1575.

[10]Yang, H., "An Artificial Compression Method for ENO Schemes: The Slope Modification Method," *Journal of Computational Physics*, Vol. 89, 1990, pp. 125–159.

[11]Ko, D. K., and Lee, D. J., "Development of an Efficient Fourth-Order Non-Oscillatory Scheme for Compressible Flows," *CFD Journal*, Vol. 6, No. 4, 1998, pp. 519–526.

S. Glegg
*Associate Editor*

# Shear Layer Instability Induced Separation Control

T. Terry Ng* and Yue Lang†
*University of Toledo, Toledo, Ohio 43606*

## I. Background

WHEN sufficiently removed from a solid surface, a separated boundary layer resembles a free shear layer. A free shear layer is subjected to several known instabilities. The computational study by Pierrehumber and Widnall[1] identifies two instabilities: 1) a narrow-band secondary instability, termed the *subharmonic instability*, that leads to the merging of spanwise vortices, and 2) a broadband fundamental mode instability, termed the *translative instability* by Pierrehumber and Widnall,[1] that leads to a streamwise vorticity concentration. Of the two, the subharmonic instability has been studied more extensively because of its primary role in the overall growth of a shear layer. In the present study, however, it is the translative instability that is of interest.

The computational study by Lin and Corcos[2] verified that a two-dimensional shear layer when subject to a spanwise sinusoidal perturbation will roll up into a series of steady, counter-rotating vortices. The experimental study by Lasheras et al.[3] shows that a single small three-dimensional perturbation on the splitter plate upstream of a free shear layer can lead to the formation of coherent, counter-rotating, streamwise vortices spreading across the entire layer. The scale of the vortices is comparable to that of the spanwise vortices and contributes substantially to the entrainment process.

The preceding results indicate that streamwise vortices of substantial strength can be induced in a free shear layer, and the vortices effectively transfer momentum from high-speed to low-speed streams in a steady fashion. The fluid action is thus similar to that desired of typical vortex generators. One main difference is that the vortices are generated through an instability, with the separated flow itself providing the vorticity. The input requirement and thus the interference on the base flow potentially can be significantly smaller than typical vortex generators. This potential is illustrated in the study by Lasheras et al.,[3] where a small perturbation leads to a substantial change in the flow downstream.

## II. Experiment Verifying a Separation Control Concept

An experimental study was conducted in a $3 \times 3$ ft closed-loop wind tunnel to provide preliminary experimental evidence supporting a separation control concept based on the preceding phenomenon. Although several means of boundary-layer control can

Received Feb. 13, 1998; revision received Nov. 9, 1998; accepted for publication Nov. 23, 1998. 

*Professor, Department of Mechanical Engineering. Senior Member AIAA.

†Graduate Assistant, Department of Mechanical Engineering.

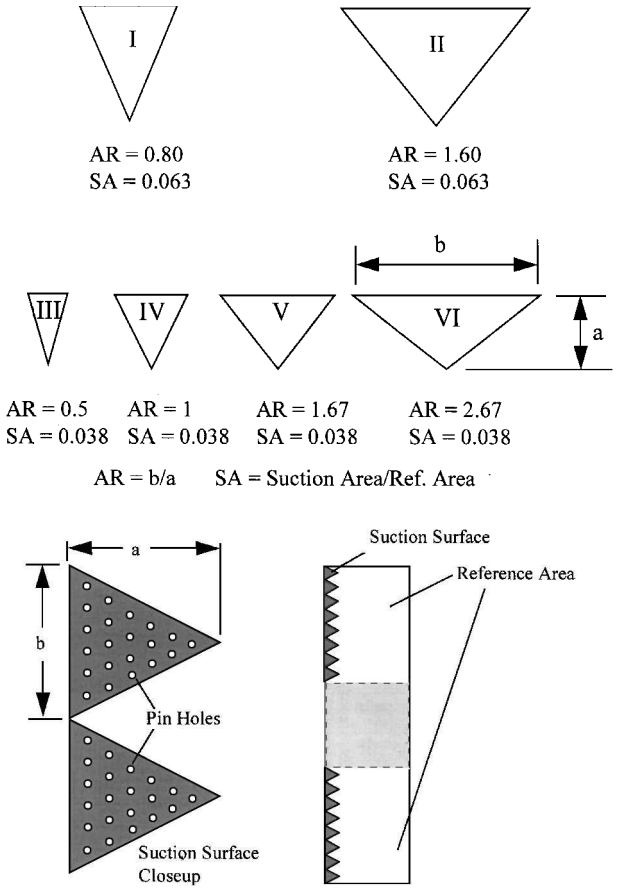


**Fig. 1 Wing model with suction.**

be used, suction is chosen for the present study primarily because of its known effectiveness and ease of application in a laboratory.

### A. Model

The model, shown in Fig. 1, is a symmetric wing with a 20% thickness. A suction surface with a spanwise, periodical distribution is implemented along the leading edge of the model. The surface consists of a metallic, porous undersurface that provides the structural strength and a removable, smooth plastic sheet that forms the outer skin. Small pin-sized holes on the plastic skin were used to create different suction patterns. A vacuum pump outside the wind tunnel provides the suction through a multistage, branching-flow network. For convenience a simple sawtooth pattern, starting at the model leading edge, was chosen to be the basic suction surface geometry. The six suction patterns shown were tested. Geometric parameters include the suction area ratio (SA) and sawtooth aspect ratio (AR).

### B. Experimental Techniques

Tests were conducted at a chord Reynolds number of $2.5 \times 10^5$ using two techniques: 1) flow visualization and 2) normal force measurement. The surface flow was visualized using fluorescent oil. The images were recorded using a video camera at a fixed position so that the images of different models at various flow conditions could be compared directly. Selected images were subsequently digitized for presentation and analysis. The normal force was measured using an internal strain gauge balance. The mechanical (spring) contribution of the suction tube to the normal force was determined with the suction on and the tunnel flow off at each combination of angle of attack and suction rate. Corrections were then applied to the flow-on data. Note that the aerodynamic force on the exposed suction tubes is included in the corrected data for the normal force. Because the exposed tubes are fairly stiff, suction did not significantly alter the geometry of the tubes. Thus, the tube aerodynamic force was assumed to be eliminated from the difference between the forces with and without suction.

The following scaling parameters will be used in the discussions of the results: $C_q$ = suction coefficient = volumetric suction rate/(freestream speed × reference area) and $\Delta C_N$ = incremental normal force (freestream dynamic pressure × reference area).

The uncertainty in the normal force measurement was estimated by repeated measurements of the model with different suction patterns (with suction turned off). Between $\alpha = 11$ deg and $\alpha = 15$ deg, stall occurs for all of the suction patterns. The precise stall angle of attack and thus the normal force behavior in this angle-of-attack range are sensitive to the variation in the leading-edge suction pattern. However, a fair consistency was revealed among different suction patterns for $\alpha$ less than 11 deg and above 15 deg. Based on the results for all of the models tested over these $\alpha$ ranges, the overall standard deviation of $\Delta C_N$ is estimated to be 0.03. This degree of uncertainty, although higher than desired for quantifying the wing performance, is deemed adequate for the purpose of providing an indication of the flow state. Furthermore, the repeatability for individual models shows a much smaller deviation, which indicates that a significant portion of the overall uncertainty is because of model-to-model variations.

### C. Results and Discussion

Without suction a stall of the wing occurs at an angle of attack of about 15 deg. The corresponding flow visualization indicates that the flow has completely separated on the leeward surface. A rather different surface flow pattern, shown in Figs. 2a and 2b, emerges when suction is applied. Figure 2a was obtained by painting uniformly with fluorescent oil a portion of the wing area aft of the suction. A series of counter-rotating vortex imprints can be seen on the surface in between triangular suction areas. The flow downstream of the vortical imprints appears to be attached. Figure 2b shows a clear picture of the vortical pattern, obtained by painting with fluorescent oil a small area in between two triangular suction areas.

Flow visualizations are subject to interpretation and often can be misleading. Thus the normal force was used as another independent indication of the state of the boundary layer. Figure 3 shows the incremental normal force due to the perturbation. At $C_q = 3.0 \times 10^{-4}$, $\Delta C_N$ increases progressively from $\alpha = 10$ deg to $\alpha = 19$ deg, which is in agreement with the deduction based on flow visualizations and again suggests that separation has been delayed because of the imposed perturbation. The values of $\Delta C_N$ are significant at high angles of attack. As shown using flow visualization in Fig. 4, the effectiveness of the control is not highly

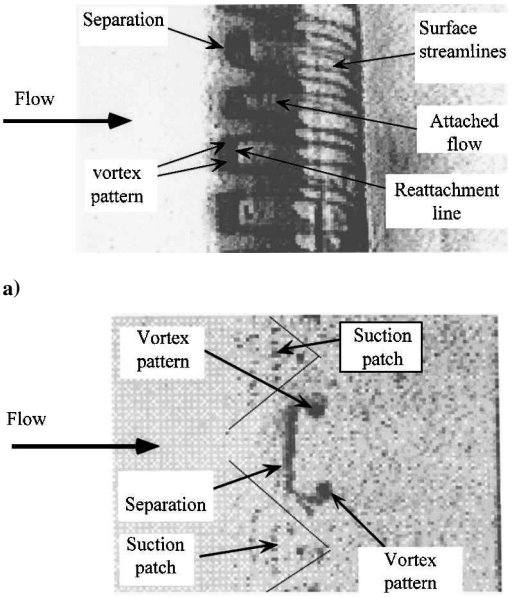


**Fig. 2 Steady-state surface flow pattern of the wing at $\alpha = 15$ deg and $C_q = 3.0 \times 10^{-4}$ for suction pattern II.**

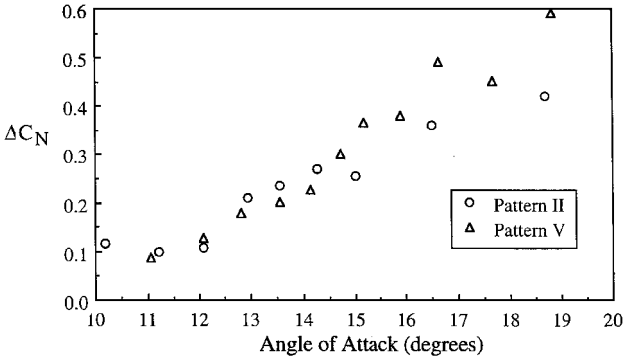


**Fig. 3 Incremental normal force coefficient at $C_q = 5.0 \times 10^{-4}$ for suction patterns II and V.**

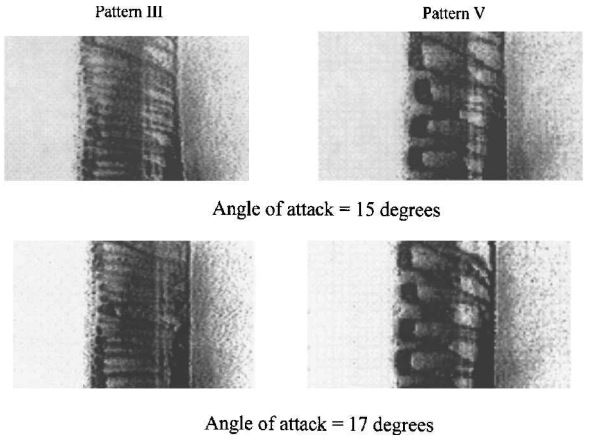


**Fig. 4 Comparison of the surface flows of patterns III and V at $C_q = 5.0 \times 10^{-4}$.**

sensitive to the suction surface geometry for a sufficiently high suction rate. This indicates that the broadband nature of the instability is retained.

## III. Conclusion

Several conclusions can be drawn from the study.

1) A periodical surface flow control can produce a three-dimensional perturbation that leads to the formation of streamwise vortical flow structures in the separated shear layer. Though suction was used in this study, boundary-layer controls in general should achieve the same effect when applied in a similar fashion.

2) The vortical structures cause a normally separated flow to reattach.

3) The control is most effective when applied near and upstream of the natural separation.

4) The control device size, as measured in this particular case by the combination of suction hole diameter, hole number density, and associated porosity, is small.

5) Similar results are obtained over different control patterns, indicating a broadband instability.

## References

[1]Pierrehumber, R. T., and Widnall, S. E., "The Two- and Three-Dimensional Instabilities of a Spatially Periodic Shear Layer," *Journal of Fluid Mechanics*, Vol. 114, 1982, pp. 59–82.

[2]Lin, S. J., and Corcos, G. M., "The Mixing Layer: Deterministic Models of a Turbulent Flow," *Journal of Fluid Mechanics*, Vol. 141, 1984, pp. 139–178.

[3]Lasheras, J. C., Cho, J. S., and Maxworthy, T., "On the Origin and Evolution of Streamwise Vortical Structures in a Plane, Free Shear Layer," *Journal of Fluid Mechanics*, Vol. 172, 1986, pp. 231–258.

A. Plotkin
*Associate Editor*

# Planar Symmetry in the Unsteady Wake of a Sphere

Rajat Mittal*
*University of Florida, Gainesville, Florida 32611*

## Introduction

THE sphere can be considered a prototypical axisymmetric bluff body, and understanding the sphere wake is important because of its relevance to a number of aerodynamic and hydrodynamic applications. In addition, vortex shedding from particles assumes importance in particulate flows at high-particle Reynolds numbers because this shedding can have a significant effect on the enhancement of turbulence.[1] In most cases particles can be modeled as spheres; therefore, an in-depth study of the vortex dynamics in sphere wakes would greatly improve our understanding of particle-turbulence interaction.

The sphere wake is nowhere as well understood as its two-dimensional counterpart, the circular cylinder, which has been the focus of intense experimental and numerical investigations in the last three decades.[2] The relatively few studies of the sphere wake that have been done to date show that the vortex topology and shedding process is significantly different from that in the cylinder wake.[3–8] Our understanding of cylinder wakes is, therefore, not directly useful in interpreting our observations of sphere wakes. In particular, there are a number of states in the steady and unsteady sphere wake that do not have a counterpart in two-dimensional wakes. These include the nonaxisymmetric steady state (or double-thread wake), which occurs at $210 < Re_d < 270$ (where $Re_d$ is the Reynolds number based on the diameter and freestream velocity), and the presence of planar symmetry in the unsteady wake regime at higher Reynolds numbers. From experiments,[3–6] stability analysis,[8] and numerical simulations,[7] it is known that the sphere wake becomes unsteady at a Reynolds number of about 270. The unsteadiness first appears as a waviness in the double-thread wake. As the Reynolds number is increased to about 290, the wavy motion gives way to vortex shedding wherein streamwise-oriented vortex loops are formed in the wake at periodic intervals.[3–6] A unique feature of the wake in this regime is that it seems to exhibit symmetry about a plane passing through the wake centerline. The presence of planar symmetry in the unsteady sphere wake is in fact peculiar enough that it is viewed by some with a degree of skepticism. This skepticism is encouraged further because of the lack of a detailed analysis of this flow regime.

The objective of the current Note is therefore to describe the salient features of this vortex shedding regime. In particular, in this Note we will 1) clearly and unequivocably establish that such a flow regime does exist, 2) describe the structure of the vortices and resultant forces on the cylinder in this regime, and 3) provide a more accurate estimate of the upper extent of this regime and an understanding of the bifurcation through which planar symmetry is lost at higher Reynolds numbers. All of these issues are addressed here through direct numerical simulations of the sphere wake.

An accurate Fourier–Chebyshev spectral collocation method has been used for computing three-dimensional, unsteady, viscous incompressible flow past a sphere. The solution is advanced in time by using a second-order-accurate, two-step, time-split scheme. The current solver has been tested extensively by performing a series of simulations of flow past a sphere in the Reynolds number range $50 < Re_d < 500$ and comparing our numerical results with established experimental data.[9] In addition to qualitative features, key quantities such as drag coefficients, separation angles, and vortex

Received March 2, 1998; revision received Nov. 18, 1998; accepted for publication Nov. 18, 1998. 

*Assistant Professor, Department of Mechanical Engineering, 237 Mechanical Engineering Building. Member AIAA.